Original scientific paper *

ELASTIC CURVE-BASED ANALYSIS FOR BENT BEAM PROFILE OPTIMIZATION

Marija Stamenković Atanasov[1], Julijana Simonović[1] and Dragan B. Jovanović[1]

[1]Faculty of Mechanical Engineering University of Niš, Serbia

Abstract. *This paper investigates the selection of cross-sectional shapes for beams based on the theory of elastic bending and the shapes of elastic curves under various forms, intensities, and distributions of loads on beams with different boundary conditions. Choosing the cross-section profile shape of a bent beam is crucial for optimizing its performance under various loading conditions. Different shapes offer varying levels of efficiency in terms of strength, stiffness, and material usage. The linear elastic theory of bending is utilized to derive the differential equation of the elastic curve for bent beams. By solving this second-order differential equation using the direct integration method and the Clebsch procedure, the elastic curves are obtained. Various loading positions and scenarios are analyzed for overhanging and cantilever elastic beams, demonstrating the correlation between beam bending stiffness, shape factor, and degree of utilization of the cross-sectional shape. We apply the criterion of ultimate bending strength (flexural strength) of steel for dimensioning beams. Thus, the characteristic dimension of the profile is determined according to the maximum value of the bending moment for each type of beam, considering the values and distribution of the load. For the same bent beam and loading values, different cross-section profiles are suggested, and the maximal deflection in each case is obtained. Based on these findings, the best choice for profile selection is considered. The study also examines the relationship between shape factors and the degree of utilization of the cross-section, and the concept of the ideal shape of beams with variable stiffness along their length. The results provide insights into the optimal selection of cross-sectional shapes for beams subjected to bending, helping engineers and designers develop a sense for the most efficient selection of cross-sectional shapes.*

Key words: *Overhanging elastic beam, Cantilever beam, Flexural rigidity, Cross-sectional shape, Bending shape factor.*

1.   INTRODUCTION

The study of beam bending and the selection of optimal cross-sectional shapes is a critical area in structural engineering, with significant implications for the design and performance of various structures. Previous research has extensively explored the theory of elastic bending and the behavior of beams under different loading conditions.

Research by Simonović et al. [1] provided a comprehensive analysis of elastic beam deformation, emphasizing the importance of integration constants in their study of elastic curves. Their work laid the groundwork for understanding the mathematical foundation of beam bending, which is crucial for our study's theoretical framework. They focused on interpreting integration constants within the framework of linear bending theory, examining their physical significance in explaining beam deformations under various loads. In engineering practice, it is crucial to comprehend the solutions generated by software that uses approximate methods. Simonović et al. aimed to connect practical engineering solutions with the underlying meaning of the results. Achieving this requires a solid physical understanding of all the terms in mathematical models and their solutions.

Building on this, Bíró et al. [2] developed a numerical method to determine the elastic curve of beams with variable cross-sections. This method is instrumental in our study, as it allows us to analyze beams with non-standard cross-sectional shapes and varying configurations. They addressed the boundary value problem by transforming it into an initial value problem using a special application of the shooting method, achieving high accuracy in obtaining the initial values of the differential equations. Their numerical results from [2] showed good agreement with analytical solutions and finite element method (FEM) results, providing a strong foundation for using modern numerical methods to derive solutions for complex loading scenarios.

Fredriksson and Mercier, in case study [3], examined material properties and structural sections, highlighting the role of shape factors in optimizing beam performance. Their findings on shape factors are crucial for our analysis of cross-sectional shapes, helping us understand the relationship between material properties and beam stiffness. They demonstrated in [3] that advanced numerical methods, such as FEM or finite difference method (FDM), simplify the problem by discretizing the beam into smaller segments or elements, making them computationally efficient and capable of handling complex geometries and loading conditions.

The significance of our research lies in its comprehensive approach to analyzing the optimal cross-sectional shapes for beams subjected to bending. By deriving the differential equation of the elastic curve and solving it for various beam configurations, we have established a clear correlation between beam bending stiffness, shape factor, and the degree of utilization of the cross-sectional shape. This study not only builds on the foundational work of previous researchers but also provides new insights into the practical application of these theories in structural design.

Our work is particularly important because it addresses the practical challenges faced by engineers and designers in selecting the most efficient cross-sectional shapes for beams. By applying the ultimate bending strength criterion for dimensioning beams, we have determined the characteristic dimensions of profiles according to the maximum

bending moment for each type of beam. This practical approach allows engineers to select the most efficient cross-sectional shapes based on real-world loading conditions.

Our current research builds on these understandings and adds new value to help engineers in their structural tasks. By providing detailed analysis and practical guidance, we aim to enhance the design and optimization of beams subjected to bending, ensuring both optimal performance and practical feasibility in structural applications.

We conducted a numerical analysis on elastic beams of varying configurations, revealing critical insights into their performance under different loading scenarios. This analysis included cantilevered beams subjected to continuous and discrete forces, as well as overhanging beams with eccentric loads. Our study demonstrates that the standard I profile is the most optimal cross-sectional shape for beams subjected to bending, offering a utilization degree that is significantly better than non-standard profiles. This finding provides practical guidance for engineers and designers in selecting the most efficient cross-sectional shapes for beams. Contrary to the traditional approach, where the material or structural element (profile) is chosen by trial method or based on previous experiences, in modern engineering, the method of multi-criteria analysis is increasingly adopted for proper and optimal selection.

The present paper begins with the theoretical foundations, introducing the fundamental concepts of bending, including pure bending and bending by forces, and discussing the criterion of ultimate bending strength for dimensioning beams. Here, we also underline the parameter that defines the efficiency of the cross-sectional area in bending. In the third section, we move on to the analytical calculation of the ideal shape of beams, focusing on the variation of the section modulus along the beam's length and the practical implications of producing beams with variable cross-sections. The fourth section contains numerical analysis, where we examine the performance of beams with various supports and loading scenarios. This section includes a series of images of elastic curves obtained using the Clebsch procedure and the tables with data on the maximum deflections of different beams, adequately suggesting the choice of standard or non-standard cross-sectional shapes. Finally, the conclusion summarizes the key findings of our study, emphasizing the importance of selecting the optimal cross-sectional shape for beams subjected to bending and providing practical guidance for engineers and designers.

By providing a detailed analysis of different cross-sectional profiles under the same loading conditions, our study offers valuable insights into the maximal deflection and the most efficient profile selection. This research not only enhances our understanding of beam bending behavior but also provides practical solutions for optimizing structural performance in various applications.

2. ELEMENTS OF ELASTIC BENDING

Bending is a type of stress characterized by the longitudinal axis or the middle line (in the case of curved beams) changing shape under the influence of load, resulting in deflection and slope relative to the initial position in the undeformed state. The shape of the curve describing the middle line of the beam in the deformed state is called the elastic curve of the beam. Mathematically, the elastic curve is the geometric locus of the deflection points $y(z)$ of the beam for the corresponding longitudinal coordinate z. The slopes are the slopes of the tangent to the elastic curve and are mathematically the first

derivatives of the function describing the elastic line $y'(z)$. The method of direct integration for obtaining the equation of elastic curves is discussed in detail in paper [1].

As in [4], we also distinguish specific cases of bending such as:

- Pure bending, where only the applied bending moment M_f causes normal stresses σ_f (Fig. 1 b) and corresponding deformations;
- Bending by forces, where transverse forces F_t cause shear stresses τ_f (Fig. 1 a), and applied moments M_f cause normal stresses σ_f (Fig. 1 b) and corresponding deformations, deflections, and slopes.
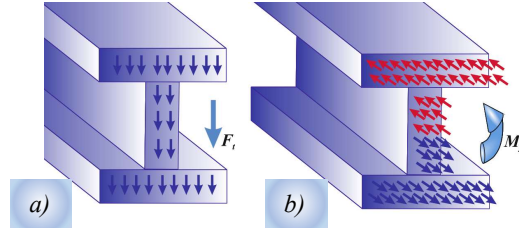

Fig. 1 Cross-sectional forces of bent profile, [4]

In the present study, we apply the criterion of the ultimate bending strength (flexural strength σ_{df}) of steel for dimensioning beams, [4]. According to this criterion, the bending stress must be less than the ultimate bending strength:

$$\sigma_z = \frac{M_{max}(z)}{W_x} \leq \sigma_{df},\tag{1}$$

where the elastic section modulus is

$$W_x[cm^3] = \frac{I_x}{y_{max}}.\tag{2}$$

We also refer to it as the bending resistance moment, and it represents the geometric characteristic of the cross-section with the dimension of length to the third power $[L^3]$, for which the units $[cm^3]$, $[mm^3]$, or $[m^3]$ can be used. From Eq. (1), it can be concluded that when dimensioning beams for bending, the bending resistance moment W_x must be greater than or equal to the ratio of the maximum bending moment $M_{max}(z)$ and the flexural strength σ_{df} for the given beam material:

$$W_x \geq \frac{|M|_{max}}{\sigma_{df}}.\tag{3}$$

The elastic section modulus W_x depends on the shape of the cross-section, with direct proportionality to the moment of inertia I_x for the axis around which the beam bends (neutral axis), and inversely proportional to the maximum distance of the edge fibers of the cross-section from the neutral axis y_{max}.

The main task of the designer when dimensioning beams is to shape a non-standard or select a standard cross-section, thereby achieving the minimum material consumption (thus the minimum weight of the structure) with economical use of labor during the construction and assembly of the structure. Most often, to achieve this, dimensioning should be done in relation to the dominant (largest) dimension of the cross-section.

Given definition (2), it can be written as:

$$W_x = \frac{1}{y_{max}} \int_A y^2 \, dA = y_{max} \int_A \left(\frac{y}{y_{max}}\right)^2 dA < y_{max} \cdot A, \tag{4}$$

since it is true for most points of the cross-section that $(y/y_{max}) < 1$.

The elastic section modulus W_x of the cross-section is equal to $W_i = y_{max} \cdot A$ only in the case when the section consists of two narrow strips (two flanges) at a distance y_{max}, which corresponds to the ideal cross-section and its ideal resistance moment W_i, as shown in Fig. 2.
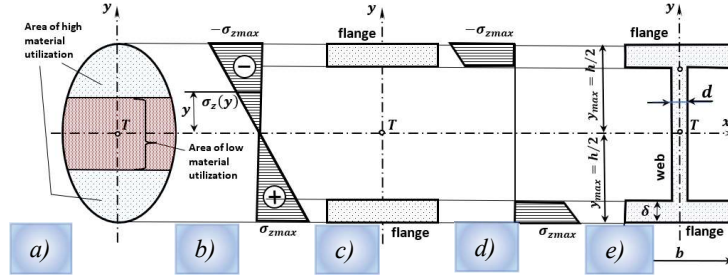

Fig. 2 a) The efficiency of the cross-sectional area in bending; b) diagram of distribution of normal stresses across the cross-section; c) the bending ideal cross-section; d) diagram of ideal distribution of normal stresses across the bending ideal cross-section; e) non-standard I profile, [4]

The ideal section modulus for the example in the figure is: $W_i = y_{max} \cdot A = \frac{1}{2} A \cdot h$. However, for the beam to be a structural unit, the flanges must be connected by a vertical web, so the actual section modulus is less than the ideal $W_x < W_i$, because it is always true for points on the web that $(y/y_{max}) < 1$. The ratio of the actual to the ideal section modulus is called the degree of utilization of the cross-section:

$$\eta = \frac{W_x}{W_i} = \frac{2 \cdot W_x}{A \cdot h} < 1. \tag{5}$$

For the non-standard I and U profiles, Fig. 3 b) and c), which have: $W_x[cm^3] = \frac{I_x}{h/2} = \frac{h^3}{6}[1 - (1 - 2\psi)^3(1 - \psi)]$, with the thickness-to-width ratio $\psi = \delta/h$, the deegre of utilization of the cross-section is:

$$\eta = \frac{W_x}{W_i} = \frac{[1 - (1 - 2\psi)^3(1 - \psi)]}{3 \cdot [1 - (1 - 2\psi)(1 - \psi)]} = 0.53 .$$

For the non-standard hollow square profiles, Fig. 3.a), which has elastic section modulus:

$$W_x[cm^3] = \frac{I_x}{h/2} = \frac{h^3}{6}[1 - (1 - 2\psi)^4], \tag{6}$$

with the thickness-to-width ratio $\psi = \delta/h = 0.2$, the deegre of utilization of the cross-section is:

$$\eta = \frac{W_x}{W_i} = \frac{[1-(1-2\psi)^4]}{3\cdot[1-(1-2\psi)^2]} = 0.453 \ .$$

Thus, we conclude that the degree of utilization is 16.97% higher for non-standard U and I profiles compared to the hollow square.
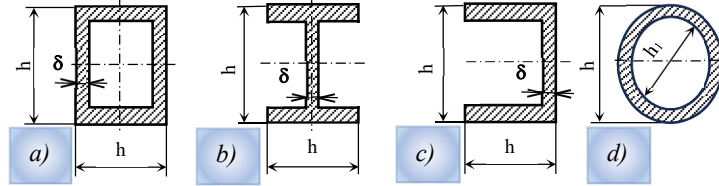

Fig. 3 Selection of non-standard profiles: a) hollow square profile; b) the I and c) U profile; d) a thin-walled tubular profile.

For a thin-walled tubular beam, cross-section in Fig. 3.d), which has $W_x[cm^3] = \frac{I_x}{h/2} = \frac{h^3\pi}{32}[1-\psi^4]$ with the radius ratio $\psi = h_1/h = 0.8$, the deegre of utilization of the cross-section ring is:

$$\eta = \frac{1-\psi^4}{4\cdot[1-\psi^2]} = 0.41 \ .$$

Thus, we conclude that the degree of utilization is 29.33% better for non-standard U and I profiles compared to the thin-walled hollow tube of the same thickness.

However, using formula (5), one can easily obtain that the standard (DIN 1026) U profile has a degree of utilization of cross-section $\eta_U = 0.595$, and the standard (DIN 1025) I profile has a value of $\eta_I = 0.64$. The standard U profile has a utilization degree that is 12.26% better than the non-standard U or I profile with η = 0.53. The standard I profile has a utilization degree that is 20.75% better than the non-standard U or I profile. The profile with the best utilization degree of the cross-section is the standard I profile, making it the preferred choice.

When selecting the most favorable profile, the degree of utilization of the profile cross-section actually provides the characteristic of the best distribution of the cross-sectional area in relation to the neutral axis, the axis around which bending occurs. Ideally, the distant flanges, Fig. 2 c), from the axis around which the beam bends are the best in terms of dimensioning the beam according to the criterion of ultimate bending strength.

Other criteria can also be used for dimensioning. For example, the allowable maximum deflection value can also be decisive. Since the deflection value is inversely proportional to the bending stiffness (flexural rigidity) of the beam, beams with greater stiffness will perform better in dimensioning. They will have a smaller deflection value for the same load. In this sense, it is appropriate to define the shape factor for elastic bending, which gives the ratio of the stiffness of profiles made of the same materials to the stiffness of a solid circular cross-section profile.

For a circular cross-section with radius r, the axial moment of inertia about the axis around which the beam bends is given by: $I_{x\odot} = \pi r^4/4 = A^2/4\pi$.

If $\mathcal{B}$ is the stiffness for another shape with the same cross-sectional area, made of the same material and subject to the same loading, then the shape factor for elastic bending is defined as:

$$\phi_f = \frac{\mathcal{B}}{\mathcal{B}_\odot} = \frac{E\,I_x}{EI_{x\odot}} = 4\pi \frac{I_x}{A^2}\,. \tag{7}$$

The shape factor ϕ_f is dimensionless, meaning it is a pure number that characterizes the cross-sectional shape relative to a circular cross-section. In practice, the shape factors range from around 1 up to around 100. Note that the size of the section (A) does not affect the shape factor if scaled proportionally. Here, a solid circular cross-section is taken as the reference shape, but the shape factor can also be considered with a solid square cross-section as the reference:

$$\phi_f = \frac{\mathcal{B}}{\mathcal{B}_\square} = \frac{E\,I_x}{EI_{x\square}} = 12\frac{I_x}{A^2}\,. \tag{8}$$

The shape factor during elastic bending of a square cross-section relative to a circular cross-section of the same area is:

$$\phi_f = \frac{I_{x\square}}{I_{x\odot}} = \frac{A^2/12}{A^2/4\pi} = \frac{4\pi}{12} = 1.05.$$

Therefore, a square cross-section is about 5% stiffer than a circular cross-section.

For a tubular beam with radius r and wall thickness δ where $r \gg \delta$, the area is $A = 2\pi r\delta$ and axial moment is $I_{x\odot} = \pi r^3 \delta$, thus the shape factor during elastic bending of a tubular beam relative to a circular cross-section of the same area is:

$$\phi_f = \frac{I_{x\odot}}{I_{x\odot}} = 4\pi \frac{\pi r^3 \delta}{(2\pi r\delta)^2} = \frac{r}{\delta}\,.$$

Therefore, a thin-walled tubular beam with $r = 10\delta$ is 10 times stiffer than a circular cross-section beam of the same area. The same applies to an I-beam. Instead of a square beam, it is approximately 10 times more efficient in bending stiffness [3]. By using the definition of ϕ_f and the values of I_x and A for the individual sections in the data-table, it is possible to plot an overview of shape factors, Fig. 4 that is taken from [3]. In Fig. 4, pultruded GFRP (Glass Fiber Reinforced Polymer) refers to a manufacturing process where continuous strands of glass fibers are impregnated with a polymer resin and then pulled through a heated die to form a composite material. This process creates strong, lightweight profiles that are used in various applications, such as construction, transportation, and industrial components. Pultruded GFRP is known for its high strength-to-weight ratio, corrosion resistance, and durability, making it an excellent choice for structural applications. Hot rolled tee sections, also known as T-bars, are structural steel profiles with a "T" shape. They are produced by hot rolling, a process where steel is heated above its recrystallization temperature and then shaped. These sections are commonly used in construction and industrial applications due to their strength and durability. The top part of the "T" (flange) provides resistance to compressive stress, while the vertical part (web) resists shear and bending forces. Hot rolled tee sections are easy to weld, cut, form, and machine, making them versatile for various projects. Also, the glulam, or glued-laminated timber, is an engineered wood

product made by bonding together layers of dimensional lumber with durable, moisture-resistant adhesives. When made from softwood species, glulam combines the natural beauty and strength of wood with enhanced structural capabilities. Softwood glulam is commonly used for beams and columns in both residential and commercial construction. It is known for its high strength-to-weight ratio, making it suitable for long spans and heavy loads. Additionally, glulam can be manufactured in various shapes and sizes, including curved and pitched forms, allowing for versatile design applications. In Fig. 4, one can also notice the position of the shape factor for a hot rolled steel joist. It is often referred to as a Rolled Steel Joist (RSJ) or an I-beam and is a structural steel component with an 'I' or 'H' shaped cross-section. These joists are produced by heating steel above its recrystallization temperature and then shaping it through rolling processes. Hot rolled steel joists are widely used in construction and civil engineering due to their strength, durability, and ability to support heavy loads. They are commonly used in building frameworks, bridges, and other structures where high load-bearing capacity is required. The design of these joists allows them to resist bending and shear forces effectively, making them ideal for various structural applications.

Using a plot, Fig. 4, of the moment of inertia versus section area, one can compare most of the commercially available structural shapes made from different materials.

Considering the relationship given by equation (2) as well as the definitions of the degree of utilization of the cross-section (5) and the section factor (8), it is not difficult to establish a connection between these dimensionless characteristics of the cross-section:

$$\phi_f = 3 \cdot \eta \cdot \frac{h^2}{A}. \tag{9}$$

Using formula (9), or (8) one can easily obtain that the standard (DIN 1026, [5]) U profile has a section factor $\phi_{fU} = 10.385$, and the standard (DIN 1025, [5]) I profile has a value of $\phi_{fI} = 18.113$. Note that the size of the section (A) does not affect the shape factor if scaled proportionally.
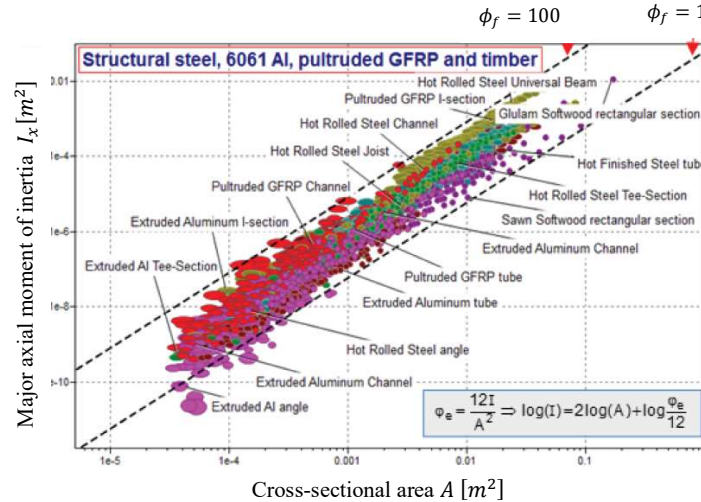

Fig. 4. An overview of shape factors [3].

Therefore, all standard profiles of the same shape have the same shape factor. Regardless of the criteria used for dimensioning the bending of the beam, this analysis shows that the standard I profile is optimal both in terms of stiffness and in terms of the utilization of the cross-sectional area.

A necessary step in optimizing bent beams is the reduction of mass, and the shape factor can be utilized in these calculations. In order to derive a performance index that includes both material and shape, we can use an I-bar in bending. Using stiffness-limited design, the authors in [3] assume a lower limit of the bending stiffness as a constraint and take as an objective to minimize mass. Taking into account both the type of material and the shape factor and optimizing the mass by using performance index, the study [3] has shown that extruded aluminum and softwood planks perform the best in that overview.

Similarly, just as the shape factor for elastic bending can be defined, Eqs. (6) or (7), the shape factor for elastic torsion can also be established. When both bending and torsion are present, the criteria for material and shape selection become more complex. This complexity allows designers to use multiple critical parameters as optimization factors.

Ultimately, the experience of the designer and the availability of material resources play a crucial role in the final selection of the profile. In conclusion, while theoretical optimization provides a strong foundation, practical considerations and the designer's expertise are essential in making the final decision. This holistic approach ensures that the selected profile meets both performance and practical requirements effectively.

In the next section, we will demonstrate the technique for selecting the ideal shape of a beam along its length. Such beams have variable stiffness along their length, and their fabrication can be demanding. Our goal is to show that the shape of the elastic line determines the ideal shape of a beam with ideal shape and variable stiffness per length.

3. IDEAL SHAPE OF BEAMS SUBJECTED TO BENDING

If a beam is subjected to transverse forces, the normal stress changes depending on the position of the cross-section as a function of the coordinate z, but it also changes at every point of the cross-section as a linear function of the coordinate y, as shown in Fig. 2 b). For a given cross-section, the largest normal stress is the edge stress. If the ideal shape of the beam is sought, then for such a beam, the edge normal stress should be equal in all cross-sections (for every z). This condition is easily met in the case of pure bending, detailed observed in [1, 4], because the bending moment is constant in every section $M_f = M = const$. In the case of a beam loaded with forces, the cross-section, i.e., its section modulus $W_x(z)$, must change so that the following relationship holds:

$$\sigma_{fmax} = \frac{M(z)}{W_x(z)} = \sigma_{df}.$$

Based on the previous expression, the criterion for dimensioning a beam of ideal shape according to the maximum bending moment and the flexural strength σ_{df} is:

$$W_x(z) = \frac{M(z)}{M_{max}} W_x = f(z). \tag{10}$$

Thus, the beam subjected to bending, having an ideal shape, has a sectional modulus that

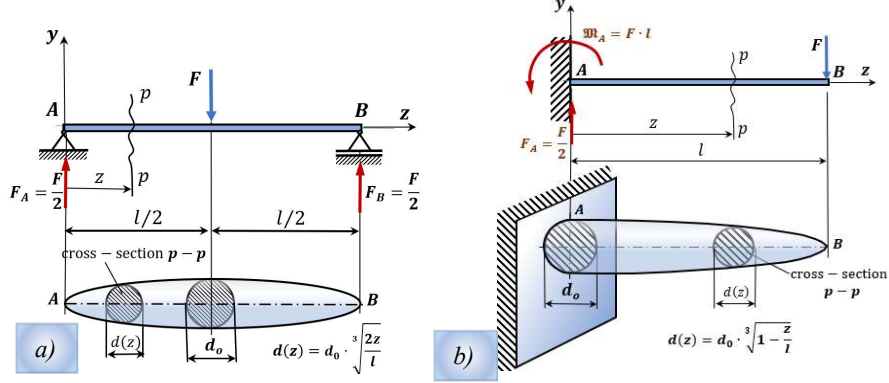varies as a function of the longitudinal z axis of the beam.

Fig. 5 Ideal shape of a) a simple beam and b) a cantilever beam of circular cross-section,
[4].

Let us consider some characteristic cases of the ideal shape: a) a simple beam with a circular cross-section loaded with a concentrated force at the middle, Fig. 4a); and b) a cantilever beam with a circular cross-section loaded with a concentrated force at the free end, Fig. 4 b).

Considering (10) the section modulus for a simple beam with a circular cross-section, Fig. 4 a), is:

$$W_x(z) = \frac{d^3(z) \cdot \pi}{32} = \frac{\frac{1}{2}F \cdot z}{\frac{1}{4}F \cdot l} \cdot \frac{d_0^3 \cdot \pi}{32},$$

from which it follows that the diameter of the cross-section changes according to the law of the cubic parabola in the case of a simple beam with a force at the middle:

$$d(z) = d_0 \cdot \sqrt[3]{\frac{2z}{l}}.$$

In the case of a cantilever beam with a circular cross-section loaded with a concentrated force at the free end, Fig. 4 b), the section modulus is given by the expression:

$$W_x(z) = \frac{d^3(z) \cdot \pi}{32} = \frac{F \cdot l\left(1 - \frac{z}{l}\right)}{F \cdot l} \cdot \frac{d_0^3 \cdot \pi}{32},$$

from which it follows that the diameter of the cross-section of the cantilever changes according to the law of the cubic parabola in the form:

$$d(z) = d_0 \cdot \sqrt[3]{1 - \frac{z}{l}}.$$

For beams with a rectangular cross-section, we choose one of the two dimensions of the rectangle, usually the larger one, to optimize it from the standpoint of the ideal shape. The production of beams with an ideal shape is demanding in terms of manufacturing technology and cost, so it is applied only in cases where it is effective.

When a beam with a variable cross-section along its length is produced, it is possible to use the same tools of elastic bending theory [1, 4] to determine the equation of the elastic curve for such beams. However, the exact solutions of the differential equation of the elastic curve for these beams are complex, so numerical tools are employed. The paper [2] presents an approach to calculating the equation of the elastic line and the code for beams with variable cross-sections along their length.

In the next chapter, we will present the results of a numerical experiment in which the elastic curves of beams with various boundary conditions and loads were obtained. These solutions were used to select the most favorable cross-sectional shape. The shapes of the elastic lines were plotted for various standard and non-standard profiles. The results and conclusions, together with the previously presented theoretical considerations, can help engineers and designers develop a sense for the most efficient selection of cross-sectional shapes for beams subjected to bending.

4. NUMERICAL RESULTS AND DISCUSSION

The examples of elastic beams examined in this section represent beams with various supports and loading scenarios. Starting with the example of a cantilevered beam subjected to continuous loading and discrete forces, followed by overhanging beams with or without eccentric axial loading, we apply the Clebsch procedure described in the papers [1, 4] to present the elastic curves for different standard and non-standard cross-sectional shapes. For all cases, we apply the criterion of the ultimate bending strength, Eq. (3), with flexural strength $\sigma_{df} = 10 \ [kN/cm^2]$ of steel for dimensioning beams. Considering the elastic section modulus (6) for non-standard hollow square profiles, Fig. 3.a), the expression for obtaining the dimension of height h becomes:

$$h[cm] \geq \sqrt[3]{\frac{6 \cdot M_{max}(z)}{\sigma_{df} \cdot [1 - (1 - 2\psi)^4]}}$$

Therefore, the characteristic dimension of the profile, specifically the height h, is determined based on the maximum value of the bending moment $M_{max}(z)$. A similar expression can be derived for the representative dimension of any other non-standard profile shown in Fig. 3. Thus, the value of the maximum bending moment $M_{max}(z)$ for each type of beam, considering the values and distribution of the load, is crucial for profile dimensioning. When dimensioning standard profiles, the same criterion and expression (3) are used. Profiles are selected from the corresponding standard tables, for example [5], choosing those with an elastic section modulus value that is the first greater than the one calculated from ratio $|M|_{max}/\sigma_{df}$. It turns out that for appropriate dimensioning, it is not only important to consider the degree of utilization of the cross-section (5) or the value of the section factor (7), but also the ratio $|M|_{max}/\sigma_{df}$. This ratio depends on the maximum value of the bending moment $M_{max}(z)$, which is determined by the type and distribution of the loading and supports, and material strength defined by

flexural strength σ_{df}. Although, as already concluded, the standard I profile with the best utilization degree of the cross-section is the preferred choice for bent beams, and some

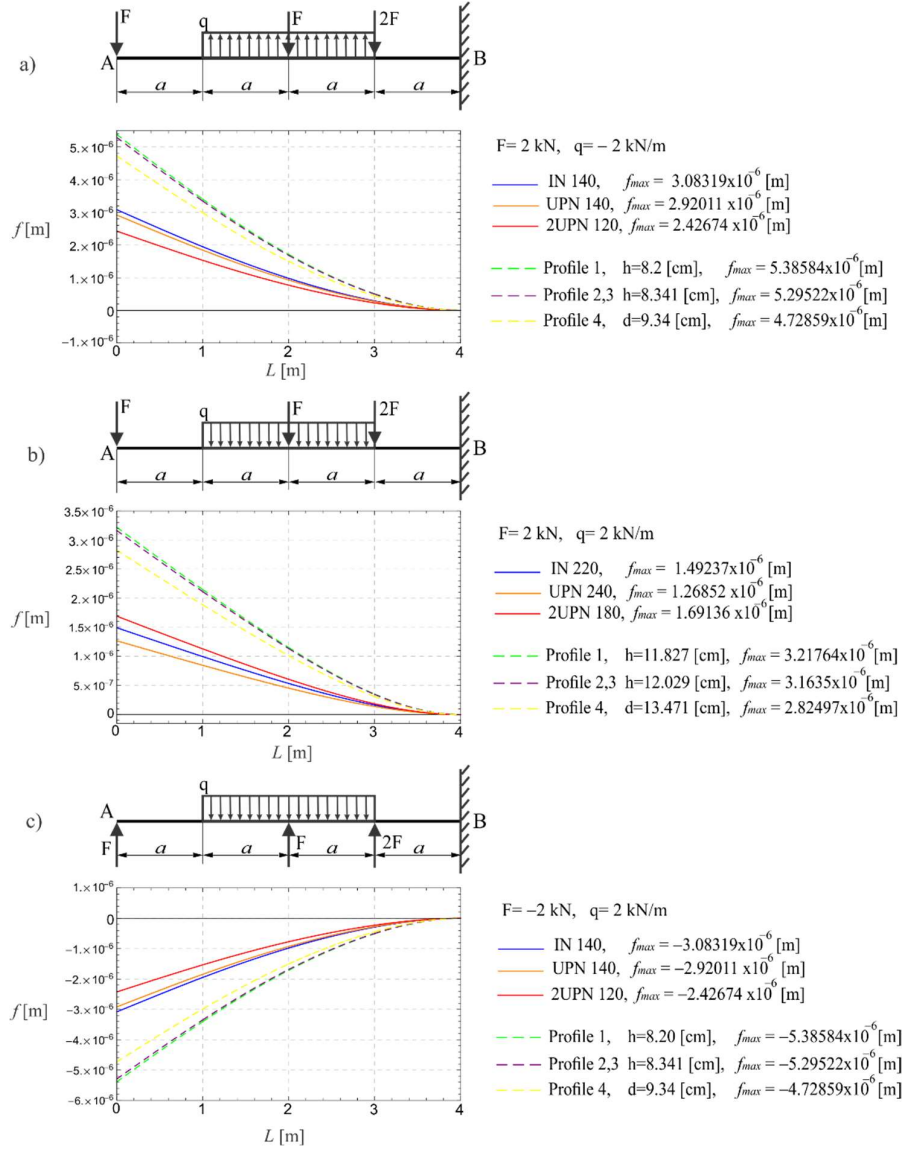**Fig. 6** The elastic curve ($y\,(z) = f\,[m]$) represents the deflection values along the cantilever beam for different scenarios of loading values and combinations. The cantilever beam has standard IN, UPN and 2UPN profiles and nonstandard profiles (1, 2,

3, 4) with $\delta/h = 0{,}2$ and total beam length of $L = 4a = 4\,[m]$

contemporary materials have high shape factors (Fig. 4), the ultimate choice of profile considers all these relations. The optimal cross-section shape can be suggested based on the knowledge of all these factors.

Once the elastic curve is obtained, the value of the maximum deflection is calculated numerically for each case and presented along with the chosen profile. This allows us to determine which of the examined profiles yields the minimal deflection values. Through such analysis, we are also able to suggest the best profile considering the minimal deflection values.

Intuitively, and as concluded in [1, 4], the orientation of the deflection depends on the direction of the applied load. So, that in all diagrams that follow in this chapter, the negative sign of deflection is mathematically below the zero axis. However, in the interpretation of deflection orientation, it is clear that negative orientations are deflections from the upper side of the zero line. Physically, this means that loads acting from top to bottom cause downward deflections, which we consider positive deformations. Deflections are actually turned upwards and represent negative values with a minus sign mathematically. Therefore, all images represent a sketch of the elastic curve, which is physically rotated 180 degrees around the zero axis. This is easy to observe in the case of a cantilever beam (Fig. 6), where we change the direction of the discrete force and continuously distributed loading.

The results from Figs. 6 and Table 1 clearly confirm that standard profiles yield lower deflection values compared to non-standard profiles, regardless of the orientation or magnitude of the load. The deflection values for standard profiles are presented with solid-colored lines in Figs. 6, while those for non-standard profiles are shown with dashed lines. Regarding non-standard profiles, a solid circular profile (Profile 4 in Table 1 and Figs. 6, yellow dashed line) shows the lowest values of deflection among all non-standard profiles. However, the deflection values for this best non-standard profile are nearly twice as high as those for standard profiles, Table 1. For standard profiles, the value of maximum deflection depends on the load orientation. In some cases, the U profile shows lower maximum deflection values, Fig. 6 b) and Table 1, while in others, the 2U profile has smaller deflection values, Figs. 6 a) and 6 c).

On the other hand, if the criterion is the lesser mass of the beam $M = \rho \cdot L \cdot A$, the profile with a lower cross-section area A is a better choice. For instance, even though profile IN220 has a maximum deflection value of $f_{max} = 1.4924\,[\mu m]$, which is greater than profile UPN 240 ($f_{max} = 1.2685\,[\mu m]$), as shown in Table 1, it has a smaller area ($A_{I220} = 39{,}5\,[cm^2]$) compared to the U profile ($A_{U240} = 42{,}3\,[cm^2]$), chosen for the same load value, beam length, and material density. Therefore, if the optimization criterion in this case is the weight of the structure, we would choose the I profile. However, if the limiting factor is the maximum deflection, we would select the U profile. As we can see, this is not a general case but only applies to this specific arrangement, direction, and type of loading, Table 1. and Fig.6 b).

How different types of loading affect the selection of the most suitable cross-section profile can be examined from Fig. 7 and Table 2. The left-hand side of Fig.7 presents a cantilever beam with only continuously distributed loading, without discrete forces, while the right-hand side shows a case with discrete forces only. For non-standard profile in

any case a solid circular profile (Profile 4 in Table 2 and Figs. 7, yellow dashed line) shows the lowest values of deflection among all non-standard profiles.

Table 1 The maximal deflection values along the cantilever beam, $(y\,(z) = f\,[m])$ for different standard and nonstandard profiles and for different scenarios of continuous loading positive values q and combinations at constant value $F=2\ [kN]$.

$F = 2\ [kN];\quad \dfrac{\delta}{h} = 0{,}2;\quad a = 1\ [m];\quad z_{max} = 0\ [m]$

q = 2 [kN/m]		q = 4 [kN/m]		q = 6 [kN/m]	
Profile	$f_{max}\,[\mu m]$	**Profile**	$f_{max}\,[\mu m]$	**Profile**	$f_{max}\,[\mu m]$
IN **220**	1.4924	IN **240**	1.4039	IN **260**	1.2834
UPN **240**	1.2685	UPN **260**	1.2379	UPN **280**	1.173
2UPN **180**	1.6914	2UPN **200**	1.5619	2UPN **220**	1.3693
for 1 $h[cm]$ 11.83	3.2176	**for 1** $h[cm]$ 13.02	2.8647	**for 1** $h[cm]$ 14.02	2.6267
for 2, 3 $h[cm]$ 12.03	3.1635	**for 2, 3** $h[cm]$ 13.24	2.8165	**for 2, 3** $h[cm]$ 14.26	2.5825
for 4 $d[cm]$ 13.47	2.8249	**for 4** $d[cm]$ 14.83	2.5151	**for 4** $d[cm]$ 15.97	2.30615

For standard profiles, the smaller value of deflection shows UPN or 2UPN profiles compared to IN profiles. However, the UPN200 profile has a smaller cross-section area ($A_{U200} = 32.2\ [cm^2]$) than the 2UPN160 ($A_{2U1} = 48\ [cm^2]$). It is worthwhile to note that for the same selected profile, the beam loaded with continuously distributed loading has smaller deflection values. As shown in Table 2, it is evident that for the same dimensions of non-standard I and U profiles (Profiles 2 and 3) with $h = 8.34[cm]$, the maximum deflection is $f_{max} = 4.19622[\mu m]$ for continuously distributed loading with a specific load per meter $q = 2[kN/m]$, Fig. 7 a), compared to $f_{max} = 4.74572\ [\mu m]$ in the case of discrete forces with a value $F = 1\ [kN]$ Fig. 7 d). Therefore, continuous load distribution is more suitable for beams subjected to bending in terms of the deformations that develop for the same dimensions and material of the beam.
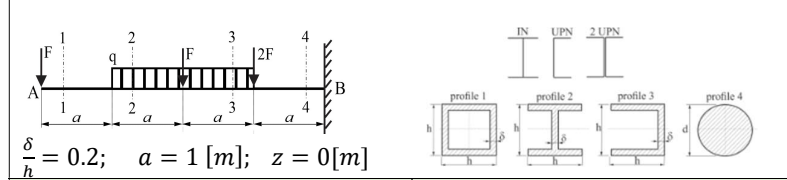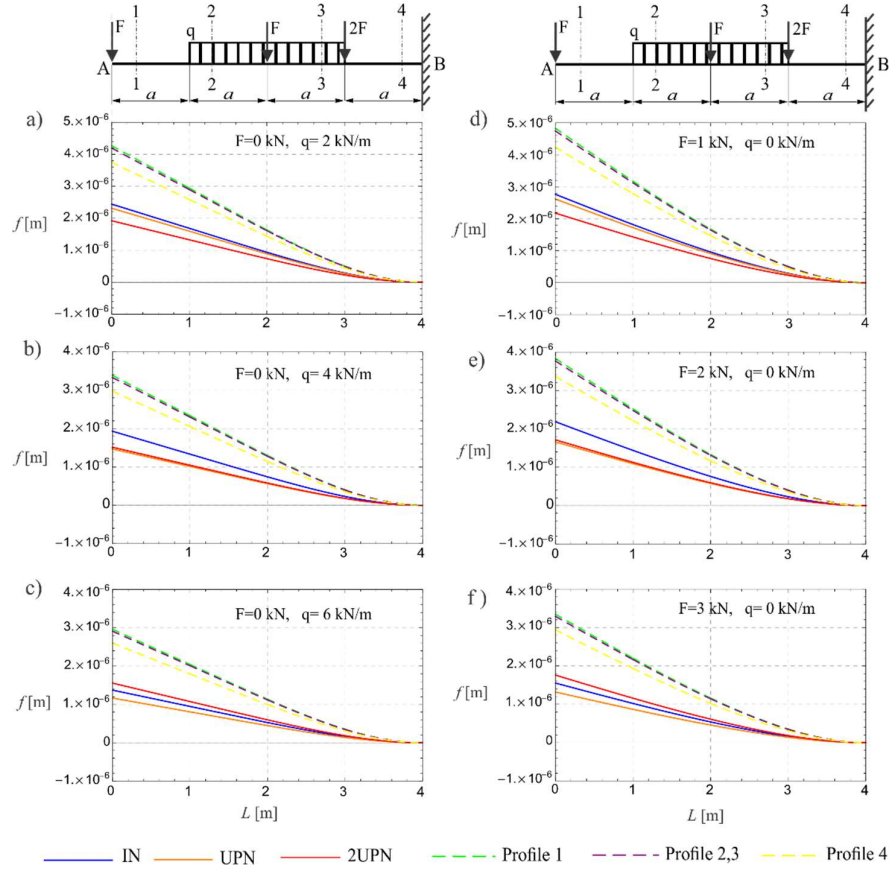
Fig. 7 The elastic curve ($y\,(z) = f\,[m]$) represents the deflection values along the cantilever beam for different scenarios of loading values and combinations $F = 0,1,2,3\,[kN]\ \ and\ \ q = 0,2,4,6[kN/m]$. The cantilever beam has standard IN, UPN and 2UPN profiles and nonstandard profiles (1, 2, 3, 4) with $\delta/h = 0{,}2\ \ and\ \ a = 1\,[m]$.

Table 2 The maximal deflection values along the cantilever beam, $(y\ (z) = f\ [m])$ for different standard and nonstandard profiles and for different scenarios of loading values and combinations $F = 0,1,2,3\ [kN]$ and $q = 0,2,4,6 [kN/m]$.

$\frac{\delta}{h} = 0.2;\quad a = 1\ [m];\quad z = 0 [m]$

Fig. 7 a) $F = 0\ [kN]$; $q = 2\ [kN/m]$		Fig. 7 d) $F = 1\ [kN]$; $q = 0\ [kN/m]$	
Profile	$f_{max}\ [\mu m]$	**Profile**	$f_{max}\ [\mu m]$
IN **140**	2.44328	IN **140**	2.76323
UPN **140**	2.31405	UPN **140**	2.61708
2UPN **120**	1.92308	2UPN **120**	2.17491
for 1 $h = 8.20 [cm]$	4.26803	**for 1** $h = 8.20 [cm]$	4.82694
for 2,3 $h = 8.34 [cm]$	4.19622	**for 2,3** $h = 8.34 [cm]$	4.74572
for 4 $d = 9.34 [cm]$	3.74718	**for 4** $d = 9.34 [cm]$	4.23788
Fig. 7 b) $F = 0\ [kN]$; $q = 4\ [kN/m]$		Fig. 7 e) $F = 2\ [kN]$; $q = 0\ [kN/m]$	
Profile	$f_{max}\ [\mu m]$	**Profile**	$f_{max}\ [\mu m]$
IN **180**	1.93103	IN **180**	2.18391
UPN **200**	1.46597	UPN **200**	1.65794
2UPN **160**	1.51351	2UPN **160**	1.71171
for 1 $h = 10.33 [cm]$	3.38754	**for 1** $h = 10.33 [cm]$	3.83114
for 2,3 $h = 10.51 [cm]$	3.33054	**for 2,3** $h = 10.51 [cm]$	3.76668
for 4 $d = 11.77 [cm]$	2.97414	**for 4** $d = 11.77 [cm]$	3.36361
Fig. 7 c) $F = 0\ [kN]$; $q = 6\ [kN/m]$		Fig. 7 f) $F = 3\ [kN]$; $q = 0\ [kN/m]$	
Profile	$f_{max}\ [\mu m]$	**Profile**	$f_{max}\ [\mu m]$
IN **220**	1.37255	IN **220**	1.55229
UPN **240**	1.16667	UPN **240**	1.31944
2UPN **180**	1.55556	2UPN **180**	1.75926
for 1 $h = 11.83 [cm]$	2.95929	**for 1** $h = 11.83 [cm]$	3.34681
for 2,3 $h = 12.03 [cm]$	2.90949	**for 2,3** $h = 12.03 [cm]$	3.2905
for 4 $d = 13.47 [cm]$	2.59815	**for 4** $d = 13.47 [cm]$	2.93838

From engineering practice, it is almost a rule that for cantilever beams, the maximum deflection occurs at the free end of the cantilever. However, in the next example (Figs. 8 d), 8 e), we show that with small changes in the intensity of the uniformly distributed load, the values of the maximum deflection do not necessarily have to be at the free end, but somewhere along the span of the beam at the value $z_{max} [m]$. For greater values of the load, the maximum deflection moves closer to the end of the cantilever, Figs. 8 d) and 8 e), and Table 3.
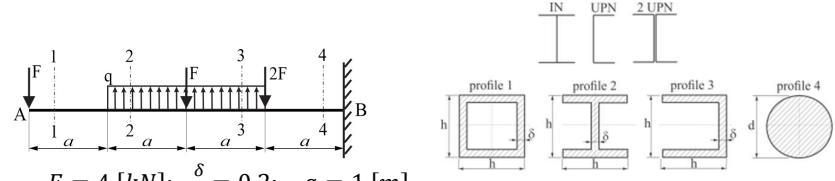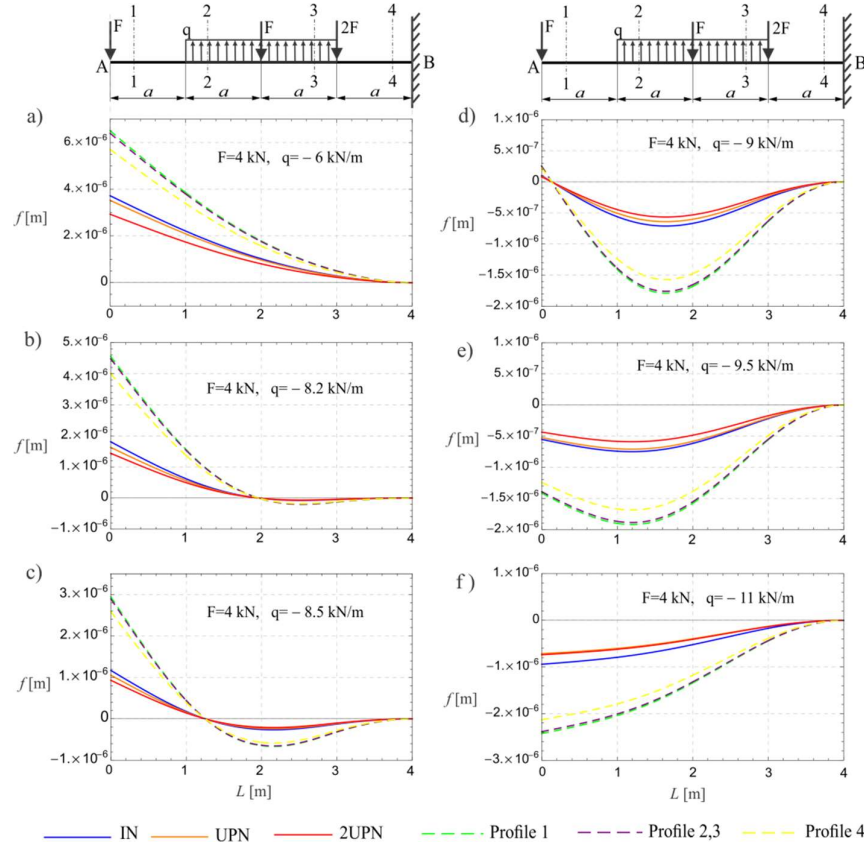
Fig. 8 The elastic curve ($y\,(z) = f\,[m]$) of the cantilever beam for different scenarios of continuous and combinations loading negative values q at constant value $F = 4\,[kN]$. The cantilever beam has a standard IN, UPN and 2UPN profiles and nonstandard profiles (1, 2, 3, 4) with $\delta/h = 0{,}2\ and\ a = 1\,[m]$.

Additional observation can be drawn from Fig. 8 and Table 3: the deflection values differ slightly among various standard profiles, but there are significant differences in the deflection values between standard and non-standard profiles. Understandably, non-standard profiles exhibit much greater deformation, with the least deformation occurring in the heaviest solid circular profile.

Engineering experience in optimal profile selection involves considering numerous factors, and the knowledge level of the designer must be substantial. In previous examples with a cantilever beam, concentric and continuous loads were observed. However, in practice, there are often eccentric axial loads that induce a reduction couple, i.e., the effect of a concentric moment. Therefore, the next examples of beams with overhangs consider the presence of such loading. Controlling the deflection magnitude through a single parameter is almost linear when considering eccentricity.

Table 3 The maximal deflection values along the cantilever beam, ($y\,(z) = f\,[m]$) for different standard and nonstandard profiles and for different scenarios of continuous and combinations loading negative values q at constant value $F = 4\,[kN]$.

$F = 4\,[kN]$; $\dfrac{\delta}{h} = 0{,}2$; $a = 1\,[m]$

Fig.8 a) $q = -6\,[kN/m]$		Fig.8 d) $q = -9\,[kN/m]$	
Profile	$f_{max}\,[\mu m]$ for $z_{max} = 0[m]$	**Profile**	$f_{max}\,[\mu m]$ for $z_{max} = 1.643[m]$
IN **140**	3.72309	IN **120**	-0.709701
UPN **140**	3.52617	UPN **120**	-0.639511
2UPN **120**	2.9304	2UPN **100**	-0.565005
for 1 $h = 8.2[cm]$	6.50366	**for 1** $h = 6.51[cm]$	-1.78822
for 2, 3 $h = 8.34[cm]$	6.39423	**for 2, 3** $h = 6.62[cm]$	-1.75814
for 4 $d = 9.34[cm]$	5.70999	**for 4** $d = 7.41[cm]$	-1.57
Fig.8 b) $q = -8.2\,[kN/m]$		Fig.8 e) $q = -9.5\,[kN/m]$	
Profile	$f_{max}\,[\mu m]$ for $z_{max} = 0[m]$	**Profile**	$f_{max}\,[\mu m]$ for $z_{max} = 1.193[m]$
IN **120**	1.80894	IN **140**	-0.748874
UPN **120**	1.63004	UPN **140**	-0.709264
2UPN **100**	1.44013	2UPN **120**	-0.589429
for 1 $h = 6.51[cm]$	4.55797	**for 1** $h = 7.45[cm]$	-1.91976
for 2, 3 $h = 6.62[cm]$	4.48128	**for 2, 3** $h = 7.58[cm]$	-1.88746
for 4 $d = 7.41[cm]$	4.00174	**for 4** $d = 8.49[cm]$	-1.68548
Fig.8 c) $q = -8.5\,[kN/m]$		Fig.8 f) $q = -11\,[kN/m]$	
Profile	$f_{max}\,[\mu m]$ for $z_{max} = 0[m]$	**Profile**	$f_{max}\,[\mu m]$ for $z_{max} = 0[m]$
IN **120**	1.1687	IN **180**	-0.942529
UPN **120**	1.05311	UPN **200**	-0.715532
2UPN **100**	0.930421	2UPN **160**	-0.738739
for 1 $h = 6.51[cm]$	2.94475	**for 1** $h = 9.39[cm]$	-2.42646
for 2, 3 $h = 6.62[cm]$	2.89521	**for 2, 3** $h = 9.55[cm]$	-2.38564
for 4 $d = 7.41[cm]$	2.58539	**for 4** $d = 10.69[cm]$	-2.13035

In Fig. 9, the variety of elastic curves for different standard and non-standard profiles are presented for beam with overhangs and axial eccentricity. Firstly, we vary the value of eccentric force while keeping the same eccentric distance. The effect of the local reduction couple is evident in the shape of the deflection of the elastic curve. For small changes in the value of the order of force magnitude of the fourth decimal place, the deflection value can be halved with an increase in load by selecting a profile of larger dimensions. See images Figs. 9 c) and 9d). For instance, instead of choosing profile IN80

that gives $f_{max} = 2.08155 [\mu m]$ for $F = 1.9000 [kN]$, it can be chosen profile IN100 that has $f_{max} = 0.94714 [\mu m]$ for $F = 1.9001 [kN]$, see Table 4. Thus, with this dimensioning criterion of ultimate bending strength, for a small loading increase, it may happen that the beam becomes considerably heavier. When comparing $A_{I80} = 7.57 [cm^2]$ to $A_{I100} = 10.6 [cm^2]$ it follows that the beam of IN100 profile has 40.03% greater weight than the of the same material and with the same loading of profile IN80.
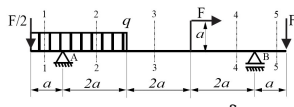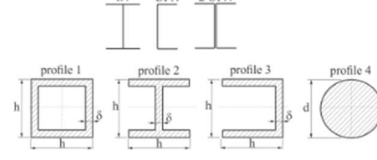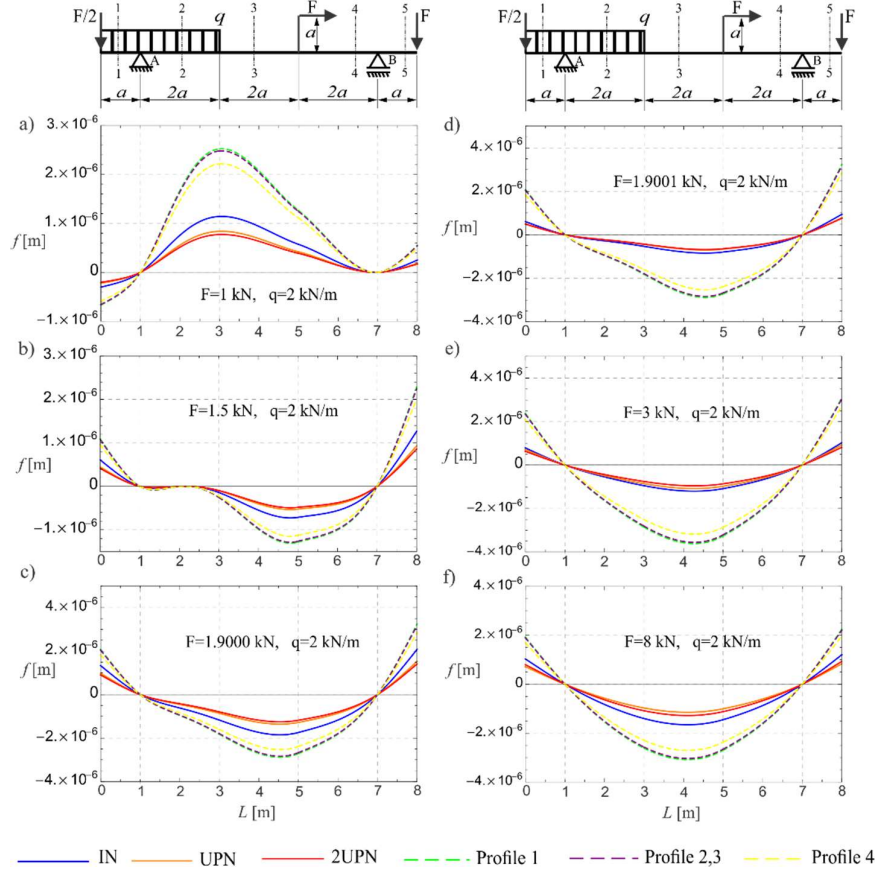

Fig. 9 The elastic curve $(y(z) = f[m])$ of a beam with axial eccentricity and distributed loading on overhang for different scenarios of distributed forces and combinations positive values F at constant continuous loading value $q = 2 [kN/m]$. The beam has a standard IN, UPN and 2UPN profiles and nonstandard profiles (1, 2, 3, 4) with $\delta/h = 0,2$ and $a = 1 [m]$.

Thus, if the optimizing criterion is reducing the weight of the beam, in this case of small variation of loading value, another criterion for dimensioning should be chosen, such as the criterion of maximum allowable deflection. Similar observations can be

deduced also from Table 5, and Figs. 10c) and 10d), which show values of maximum deflection variations with small changes in specific continuous loading $q[kN/m]$.
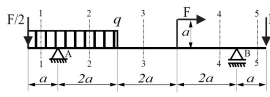
Table 4 The maximal deflection values of a beam with axial eccentricity and distributed loading on overhang $(y(z) = f[m])$, for different scenarios of distributed forces and combinations positive values F at constant continuous loading value $q = 2\ [kN/m]$.

$$q = 2\ [kN/m]\ ;\quad \frac{\delta}{h} = 0.2;\quad a = 1\ [m]$$

Fig. 9 a) $F = 1\ [kN]$		Fig. 9 d) $F = 1.9001\ [kN]$	
Profile	$f_{max}\ [\mu m]$ for $z_{max} = 3.057[m]$	**Profile**	$f_{max}\ [\mu m]$ for $z_{max} = 8.0[m]$
IN **80**	1.14354	IN **100**	0.94714
UPN **80**	0.839313	UPN **100**	0.78622
2UPN **65**	0.773627	2UPN **80**	0.76396
for 1 $h = 4.69[cm]$	2.52732	**for 1** $h = 5.12\ [cm]$	3.2426
for 2, 3 $h = 4.69[cm]$	2.4848	**for 2, 3** $h = 5.21[cm]$	3.18809
for 4 $d = 5.35[cm]$	2.2189	**for 4** $d = 5.83[cm]$	2.84693
Fig. 9 b) $F = 1.5\ [kN]$		Fig. 9 e) $F = 3\ [kN]$	
Profile	$f_{max}\ [\mu m]$ for $z_{max} = 8.0[m]$	**Profile**	$f_{max}\ [\mu m]$ for $z_{max} = 4.27[m]$
IN **80**	1.2675	IN **120**	-1.20149
UPN **80**	0.93029	UPN **120**	-1.08267
2UPN **65**	0.85749	2UPN **100**	-0.95653
for 1 $h = 4.94[cm]$	2.28084	**for 1** $h = 6.23[cm]$	-3.61735
for 2, 3 $h = 5.03[cm]$	2.24246	**for 2, 3** $h = 6.33[cm]$	-3.55649
for 4 $d = 5.63[cm]$	2.0025	**for 4** $d = 7.09\ [cm]$	-3.17591
Fig. 9 c) $F = 1.9000\ [kN]$		Fig. 9 f) $F = 8\ [kN]$	
Profile	$f_{max}\ [\mu m]$ for $z_{max} = 8.00[m]$	**Profile**	$f_{max}\ [\mu m]$ for $z_{max} = 4.099[m]$
IN **80**	2.08155	IN **160**	-1.65561
UPN **80**	1.52778	UPN **180**	-1.14666
2UPN **65**	1.40821	2UPN **140**	-1.27933
for 1 $h = 5.12[cm]$	3.24244	**for 1** $h = 9.12[cm]$	-3.08649
for 2, 3 $h = 5.21[cm]$	3.18789	**for 2, 3** $h = 9.27[cm]$	-3.03456
for 4 $d = 5.83[cm]$	2.84675	**for 4** $d = 10.39[cm]$	-2.70983

It is interesting to note that while standard profiles change their dimensions and increase the overall size of the structure for such small changes in loading, both force (Fig. 9 and Table 4) and continuous loading (Fig. 10 and Table 5), the dimensions of non-standard profiles do not change (see Tables 4 for $F = 1.9000[kN]$ and $F = 1.9001[kN]$ and Table 5 for $q = 4.8400\ [kN/m]$ and $q = 4.8401\ [kN/m]$). From this, we conclude that although non-standard profiles have in general higher deflection values, they

maintain these values over a wider range of loading changes, making them more robust to small variations in loading values.

Table 5 The maximal deflection values of a beam with axial eccentricity and distributed loading on overhang ($y\,(z) = f\,[m]$), for different scenarios of continuous and combinations loading positive values q at constant value $F = 2\,[kN]$.

$F = 2\,[kN];\quad \dfrac{\delta}{h} = 0.2;\quad a = 1\,[m]$

Fig. 10 a) $q = 2\,[kN/m]$		Fig. 10 d) $q = 4.8401[kN/m]$	
Profile	$f_{max}\,[\mu m]$ for $z_{max} = 8.00[m]$	**Profile**	$f_{max}\,[\mu m]$ for $z_{max} = 3.24[m]$
IN **100**	1.03964	IN **120**	0.92295
UPN **100**	0.86299	UPN **120**	0.83167
2UPN **80**	0.83857	2UPN **100**	0.73477
for 1 $h = 5.17[cm]$	3.44131	**for 1** $h = 6.18[cm]$	2.86568
for 2, 3 $h = 5.25[cm]$	3.3834	**for 2, 3** $h = 6.28[cm]$	2.81746
for 4 $d = 5.89[cm]$	3.02135	**for 4** $d = 7.04[cm]$	2.51597
Fig. 10 b) $q = 3\,[kN/m]$		Fig. 10 e) $q = 8\,[kN/m]$	
Profile	$f_{max}\,[\mu m]$ for $z_{max} = 8.00[m]$	**Profile**	$f_{max}\,[\mu m]$ for $z_{max} = 3.47[m]$
IN **100**	0.63353	IN **140**	1.36935
UPN **100**	0.52589	UPN **140**	1.29693
2UPN **80**	0.51101	2UPN **120**	1.0778
for 1 $h = 5.56[cm]$	1.55738	**for 1** $h = 7.61[cm]$	3.22724
for 2, 3 $h = 5.66[cm]$	1.53118	**for 2, 3** $h = 7.74[cm]$	3.17294
for 4 $d = 6.34[cm]$	1.36733	**for 4** $d = 8.67[cm]$	2.83341
Fig. 10 c) $q = 4.8400\,[kN/m]$		Fig. 10 f) $q = 10\,[kN/m]$	
Profile	$f_{max}\,[\mu m]$ for $z_{max} = 3.24[m]$	**Profile**	$f_{max}\,[\mu m]$ for $z_{max} = 3.52[m]$
IN **100**	1.77025	IN **160**	1.16803
UPN **100**	1.46948	UPN **180**	0.80896
2UPN **80**	1.42789	2UPN **140**	0.90256
for 1 $h = 6.18[cm]$	2.86559	**for 1** $h = 8.35[cm]$	3.0951
for 2, 3 $h = 6.28[cm]$	2.81738	**for 2, 3** $h = 8.49[cm]$	3.04302
for 4 $d = 7.04[cm]$	2.51589	**for 4** $d = 9.51[cm]$	2.71739

Additionally, this example of a beam with eccentric loading, as shown in Figs. 9 and 10 and Tables 4 and 5, provides clear illustrations that highlight the effect of eccentricity on the location of maximum deflection. For small changes in loading values, this location shifts along the beam much more than in the example with a cantilever beam without eccentricity.
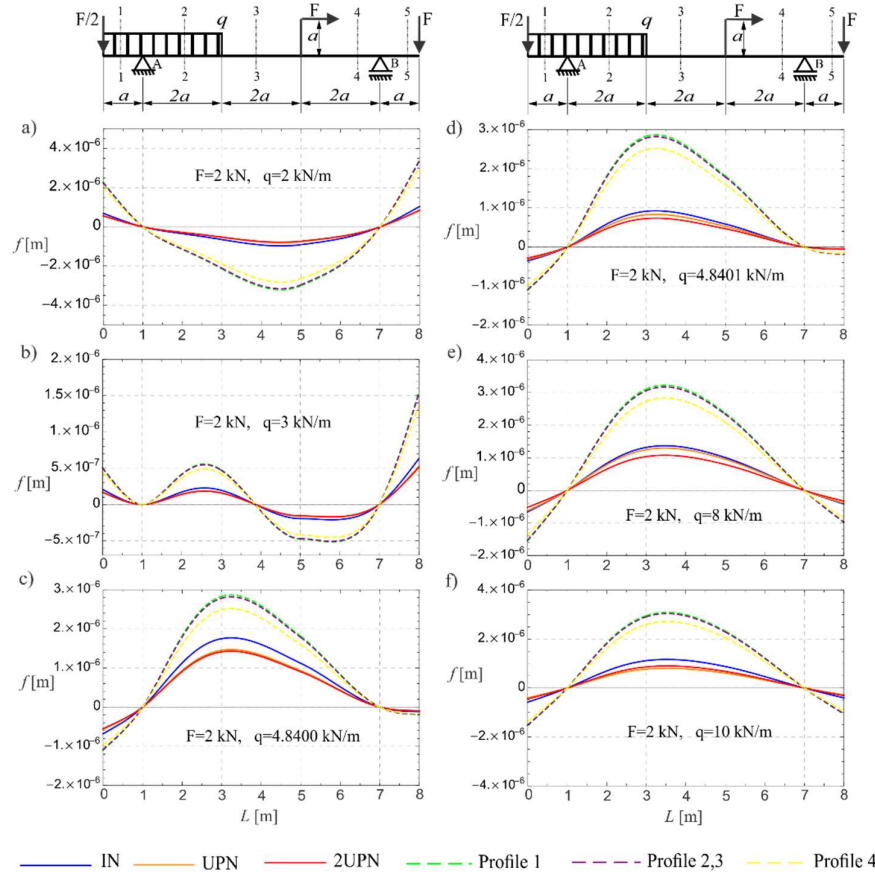
Fig. 10 The elastic curve ($y(z) = f[m]$) of a beam with axial eccentricity and distributed loading on overhang for different scenarios of continuous and combinations loading positive values q at constant value $F = 2\ [kN]$. The beam has a standard IN, UPN and 2UPN profiles and nonstandard profiles (1, 2, 3, 4) with $\delta/h = 0{,}2\ and\ a = 1\ [m]$.

If there is eccentric loading, the deflection magnitude and profile shape can be controlled by the eccentric distance $r\ [m]$ from the beam's axis. Thus, Fig. 11 shows the shape of the elastic curve with changes in the length of eccentricity. Table 6 accompanies this figure and shows the maximum deflection values and the characteristic cross-sections where these values occur for the selected profiles. For the beam with overhangs shown in Fig. 11, also in Figs. 9 and 10, we observe that the maximum deflection most often occurs at the right overhang, but the maximum deflection value can also be between the supports. When the distance of the eccentric axial force from the beam's axis $r\ [m]$ increases, we control the occurrence of maximum deflection, which now appears between the supports rather than at the free end, Figs. 11 e) and 11 f), and Table 6.
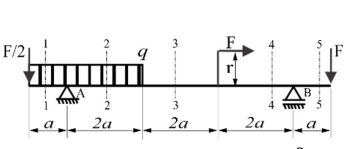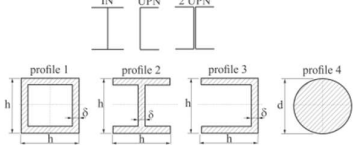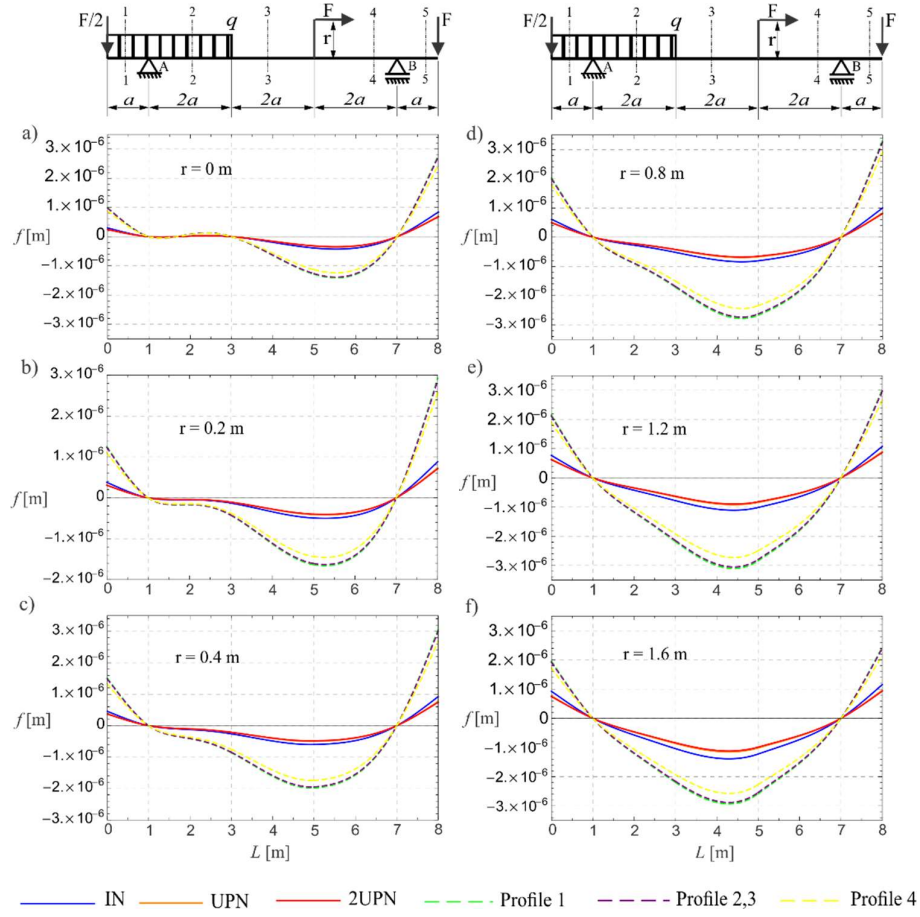
Fig. 11 The elastic curve ($y\,(z) = f[m]$) of a beam with axial eccentricity and distributed loading on overhang for different scenarios of combination impact of eccentricity distance $r\,[m]$ and constant values of loading $F = 2\,[kN]$ and $q = 2\,[kN/m]$. The beam has a standard IN, UPN and 2UPN profiles and nonstandard profiles (1, 2, 3, 4) with $\delta/h = 0{,}2$ and $a = 1\,[m]$.

From Table 6, it is evident that increasing the eccentricity distance $r\,[m]$ linearly increases the deflection at specific points $z\,[m]$ along the beam. This linear trend is shown in Fig. 12 for the standard IN 100 profile and applies to any selected profile, whether standard or non-standard. This means that the deflection value can be linearly controlled by one parameter, specifically the increase in eccentricity distance.

Table 6 The maximal deflection values of a beam with axial eccentricity and distributed loading on overhang, for different scenarios of combination impact of eccentricity distance $r\ [m]$ and constant values of loading $F = 2\ [kN]$ and $q = 2\ [kN/m]$.

$F = 2\ [kN];\quad q = 2[kN/m];\quad \dfrac{\delta}{h} = 0.2;\quad a = 1\ [m]$

Fig. 11 a) $r = 0\ [m]$		Fig. 11 d) $r = 0.8\ [m]$	
Profile	$\boldsymbol{f_{max}}\ [\boldsymbol{\mu m}]$ for $z = 8.00\ [m]$	**Profile**	$\boldsymbol{f_{max}}\ [\boldsymbol{\mu m}]$ for $z = 8.00\ [m]$
IN **100**	0.84470	IN **100**	1.00065
UPN **100**	0.70119	UPN **100**	0.83064
2UPN **80**	0.68134	2UPN **80**	0.80713
for 1 $h = 5.17[cm]$	2.79606	**for 1** $h = 5.17[cm]$	3.31226
for 2, 3 $h = 5.25[cm]$	2.74902	**for 2, 3** $h = 5.25[cm]$	3.25653
for 4 $d = 5.88[cm]$	2.45485	**for 4** $d = 5.88[cm]$	2.90805
Fig. 11 b) $r = 0.2\ [m]$		Fig. 11 e) $r = 1.2\ [m]$	
Profile	$\boldsymbol{f_{max}}\ [\boldsymbol{\mu m}]$ for $z = 8.00\ [m]$	**Profile**	$\boldsymbol{f_{max}}\ [\boldsymbol{\mu m}]$ for $z = 4.407\ [m]$
IN **100**	0.88369	IN **100**	-1.10832
UPN **100**	0.73354	UPN **100**	-0.92001
2UPN **80**	0.71278	2UPN **80**	-0.89397
for 1 $h = 5.17[cm]$	2.92511	**for 1** $h = 5.39[cm]$	-3.10477
for 2, 3 $h = 5.25[cm]$	2.87589	**for 2, 3** $h = 5.48[cm]$	-3.05253
for 4 $d = 5.88[cm]$	2.56815	**for 4** $d = 6.13[cm]$	-2.72588
Fig. 11 c) $r = 0.4\ [m]$		Fig. 11 f) $r = 1.6\ [m]$	
Profile	$\boldsymbol{f_{max}}\ [\boldsymbol{\mu m}]$ for $z = 8.00\ [m]$	**Profile**	$\boldsymbol{f_{max}}\ [\boldsymbol{\mu m}]$ for $z = 4.288[m]$
IN **100**	0.92267	IN **100**	-1.38676
UPN **100**	0.76591	UPN **100**	-1.15115
2UPN **80**	0.74423	2UPN **80**	-1.11857
for 1 $h = 5.17[cm]$	3.05416	**for 1** $h = 5.78[cm]$	-2.93094
for 2, 3 $h = 5.25[cm]$	3.00277	**for 2, 3** $h = 5.88[cm]$	-2.88163
for 4 $d = 5.88[cm]$	2.68145	**for 4** $d = 6.58[cm]$	-2.57327

To meet a deflection limit, the designer can reduce the distance of the eccentric axial force while keeping other beam parameters constant. This approach ensures the required deflection value in a straightforward, linear prediction manner.
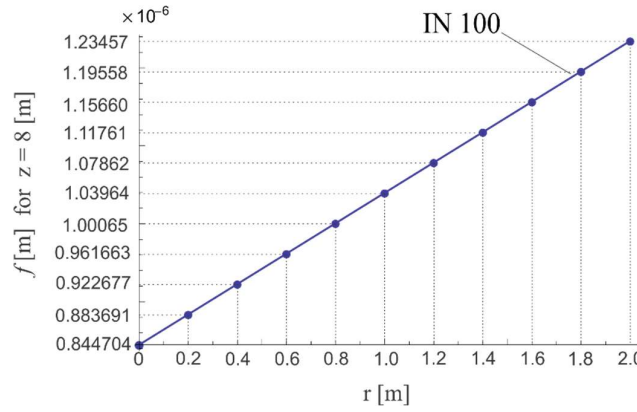
Fig. 12 Deflection diagram of a beam with an overhang at the free end for $z = 8\ [m]$, depending on the eccentric distance from the longitudinal axis of the beam $r\ [m]$ of the force $F = 2\ [kN]$. For $q = 2\ [kN/m]$, $\delta/h = 0{,}2$ and $a = 1\ [m]$ the beam is a standard IN 100 profile.

All previously made conclusions regarding the selection of profiles and the values of maximum deflections for overhang beams with eccentricity can also be applied to the following example of an overhang beam without axial eccentricity. Fig. 13 illustrates the different shapes of the elastic curve under varying values and orientations of continuously distributed loading. If the orientation of the concentrated forces remains unchanged while only the orientation of the continuous loading varies, the direction of the deflection changes accordingly. This can be observed by comparing the right and left-hand sides of Fig. 13. In this case, it is confirmed that among non-standard profiles, the solid circular cross-section yields the lowest deflection value under the same load, but it also has the lowest surface utilization efficiency (the degree of utilization of the cross-section η). Regarding standard profiles with much higher surface utilization efficiency, standard U or 2U profiles prove to be better than I profile in terms of lower deflection values, as shown in Table 7. However, as previously commented, double U profiles have a lower shape factor ϕ_f and are less favorable in terms of the weight-to-load-bearing ratio.

The elastic curves shown in Fig. 14 and the results in Table 8 demonstrate that the deflection between supports can be adjusted and controlled by varying the orientation and relationship between discrete forces on the overhangs. Regarding the selection of profiles, the same conclusions as before can be applied to this type of beam and load distribution. Generally, as the magnitude of the load increases, larger profile dimensions are required. For the same load and selected profile based on the ultimate bending strength criterion, standard profiles yield significantly lower absolute deflection values compared to non-standard profiles. U profiles exhibit slightly lower deflections than selected I profiles, but I profiles have smaller surface areas, making them more optimal in terms of weight-to-load ratio.
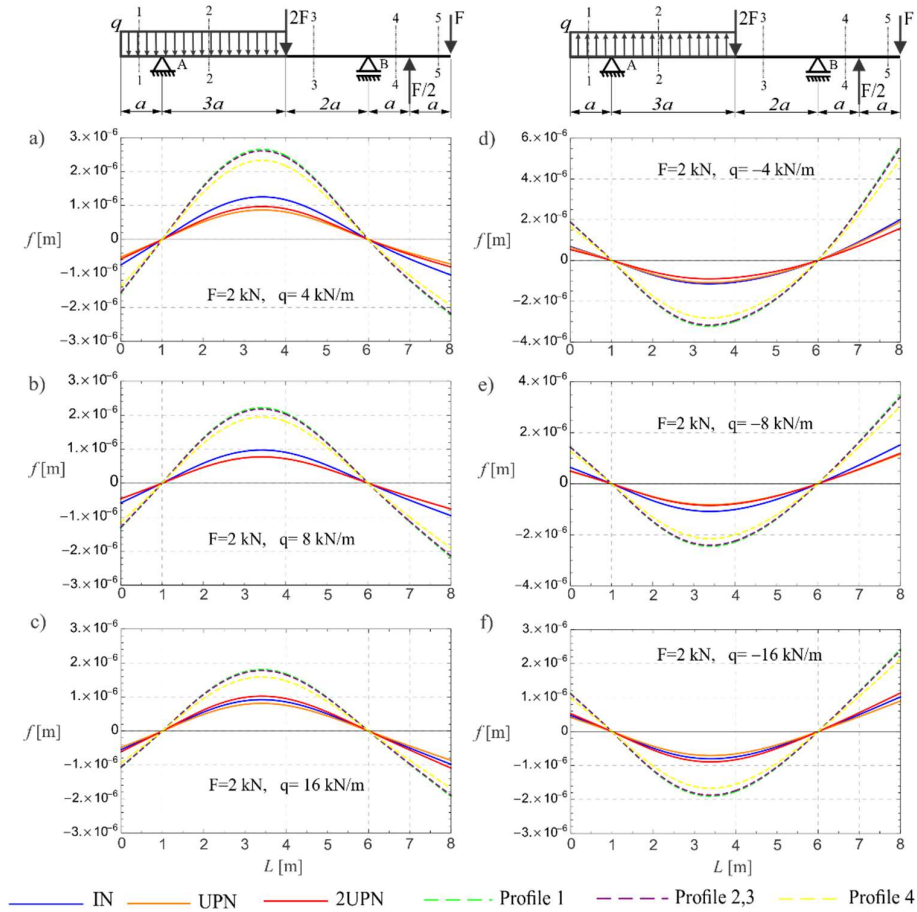
Fig. 13 The elastic curve ($y(z) = f[m]$) represents the deflection values along the beam length for different scenarios of continuous and combinations loading positive and negative values q at constant value F=2 [kN]. The beam has a standard IN, UPN and 2UPN profiles and nonstandard profiles (1, 2, 3, 4) with $\delta/h = 0{,}2 \ and \ a = 1 \ [m]$.

At the very end of the analysis, let us make a small comparison of the values of selected profiles and beam weight as the magnitude of discrete forces increases (see Fig. 15). Comparing the results from Fig. 15 a) and Fig. 15 c), it can be observed that when the magnitude of the force is multiplied by 2, 3 times (from $F = 6 \ [kN]$ to $F = 20 \ [kN]$) the profile UPN with the smallest value of maximum deflection takes standard values from UPN 200 to UPN 260. The height of the beam increases by only 6 [cm], but the section area enlarges significantly, from $A_{U200} = 32.2 \ [cm^2]$ to $A_{U260} = 48.3 \ [cm^2]$, which increases the weight of the beam made from the same material and of the same total length by 50%. Finally, the increase in the magnitude of the force necessitates a

larger profile dimension to maintain structural integrity. While the height of the beam increases slightly, the section area sees a significant enlargement, resulting in a notable increase in the weight of the beam. This adjustment ensures that the beam can handle the increased load while maintaining the desired deflection characteristics.

Table 7 The maximal deflection values of a beam with distributed loading on overhang $(y(z) = f[m])$, for different scenarios of continuous and combinations loading positive and negative values q at constant value $F = 2\ [kN]$.
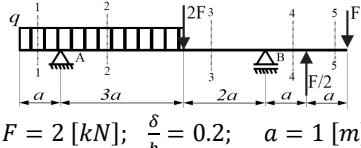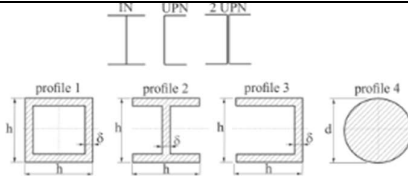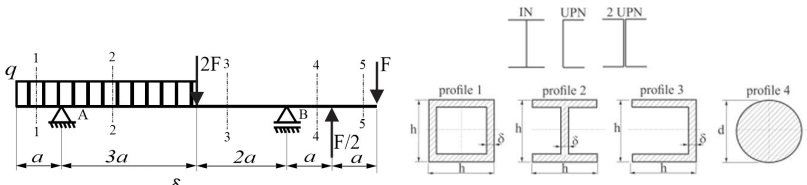

$F = 2\ [kN];\quad \frac{\delta}{h} = 0.2;\quad a = 1\ [m]$

Fig. 13 a) $q = 4\ [kN/m]$		Fig. 13 d) $q = -4\ [kN/m]$	
Profile	$f_{max}\ [\mu m]$ for $z = 3.426[m]$	**Profile**	$f_{max}\ [\mu m]$ for $z = 8.00[m]$
IN **160**	1.25314	IN **140**	2.00407
UPN **180**	0.867916	UPN **140**	1.89807
2UPN **140**	0.968337	2UPN **120**	1.57738
for 1 $h = 8.84\ [cm]$	2.65099	**for 1** $h = 7.28\ [cm]$	5.62583
for 2, 3 $h = 8.99\ [cm]$	2.60639	**for 2, 3** $h = 7.41\ [cm]$	5.53117
for 4 $d = 10.6\ [cm]$	2.3274	**for 4** $d = 8.29\ [cm]$.	4.93928
Fig. 13 b) $q = 8\ [kN/m]$		Fig. 13 e) $q = -8\ [kN/m]$	
Profile	$f_{max}\ [\mu m]$ for $z = 3.417[m]$	**Profile**	$f_{max}\ [\mu m]$ for $z = 8.00[m]$
IN **200**	0.974937	IN **180**	1.52529
UPN **220**	0.775601	UPN **200**	1.15794
2UPN **180**	0.772728	2UPN **160**	1.1955
for 1 $h = 10.67\ [cm]$	2.21915	**for 1** $h = 9.69\ [cm]$	3.45028
for 2, 3 $h = 10.85[cm]$	2.18181	**for 2, 3** $h = 9.86\ [cm]$	3.39223
for 4 $d = 12.15\ [cm]$	1.94834	**for 4** $d = 11.04\ [cm]$	3.02922
Fig. 13 c) $q = 16\ [kN/m]$		Fig. 13 f) $q = -16\ [kN/m]$	
Profile	$f_{max}\ [\mu m]$ for $z = 8.00[m]$	**Profile**	$f_{max}\ [\mu m]$ for $z = 8.00[m]$
IN **240**	-0.980784	IN **240**	1.02078
UPN **260**	-0.864799	UPN **260**	0.900069
2UPN **200**	-1.09119	2UPN **200**	1.13569
for 1 $h = 13.15\ [cm]$	-1.92465	**for 1** $h = 12.53\ [cm]$	2.42498
for 2, 3 $h = 13.37[cm]$	-1.89227	**for 2, 3** $h = 12.75\ [cm]$	2.38418
for 4 $d = 14.97\ [cm]$	-1.68978	**for 4** $d = 14.28\ [cm]$	2.12905

Table 8 The maximal deflection values of a beam with distributed loading on overhang ($y\,(z) = f\,[m]$), for different scenarios of distributed forces and combinations negative values F at constant continuous loading value $q = 4\,[kN/m]$.

$q = 4\,[kN/m]$; $\frac{\delta}{h} = 0.2$; $a = 1\,[m]$; $z = 8\,[m]$

| Fig. 14 a) $F = -2\,[kN]$		Fig. 14 d) $F = -9\,[kN]$	
Profile	$f_{max}\,[\mu m]$	**Profile**	$f_{max}\,[\mu m]$
IN **140**	-2.00407	IN **180**	-0.99713
UPN **140**	-1.89807	UPN **200**	-0.75698
2UPN **120**	-1.57738	2UPN **160**	-0.78153
for 1 $h = 7.28[cm]$	-5.62583	**for 1** $h = 9.76[cm]$	-2.19395
for 2, 3 $h = 7.41[cm]$	-5.53117	**for 2, 3** $h = 9.93[cm]$	-2.15703
for 4 $d = 8.29[cm]$	-4.93928	**for 4** $d = 11.12[cm]$	-1.92621
Fig. 14 b) $F = -6\,[kN]$		Fig. 14 e) $F = -10\,[kN]$	
Profile	$f_{max}\,[\mu m]$	**Profile**	$f_{max}\,[\mu m]$
IN **160**	-1.40998	IN **180**	-1.02644
UPN **180**	-0.97654	UPN **200**	-0.77923
2UPN **140**	-1.08953	2UPN **160**	-0.80451
for 1 $h = 8.53[cm]$	-3.43496	**for 1** $h = 10.11[cm]$	-1.96245
for 2, 3 $h = 8.67[cm]$	-3.37716	**for 2, 3** $h = 10.29\,[cm]$	-1.92943
for 4 $d = 9.71[cm]$	-3.01577	**for 4** $d = 11.52[cm]$	-1.72296
Fig. 14 c) $F = -8\,[kN]$		Fig. 14 f) $F = -16\,[kN]$	
Profile	$f_{max}\,[\mu m]$	**Profile**	$f_{max}\,[\mu m]$
IN **180**	-0.96782	IN **220**	-0.56972
UPN **200**	-0.73473	UPN **240**	-0.48426
2UPN **160**	-0.75856	2UPN **180**	-0.64568
for 1 $h = 9.39[cm]$	-2.49156	**for 1** $h = 11.83[cm]$	-1.22834
for 2, 3 $h = 9.55[cm]$	-2.44964	**for 2, 3** $h = 12.03[cm]$	-1.20767
for 4 $d = 10.69[cm]$	-2.18751	**for 4** $d = 13.47\,[cm]$	-1.07844
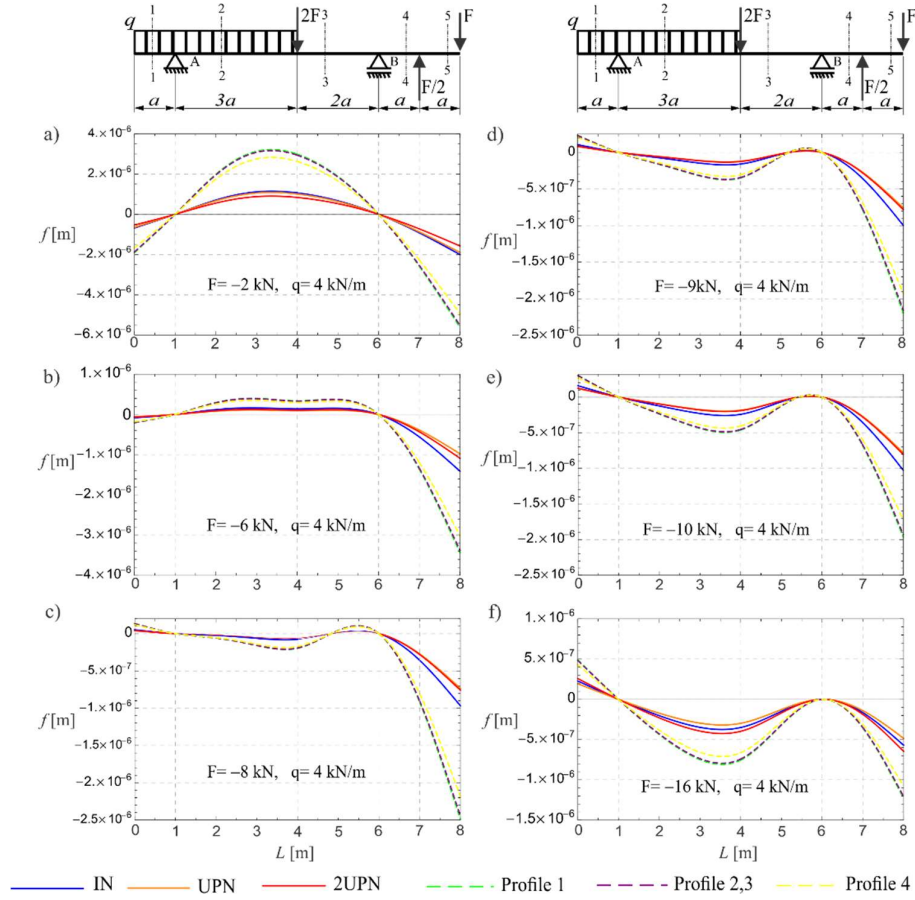
Fig. 14 The elastic curve $(y(z) = f[m])$ represents the deflection values along the beam length for different scenarios of distributed forces and combinations negative values F at constant continuous loading value $q = 4\,[kN/m]$. The beam has a standard IN, UPN and 2UPN profiles and nonstandard profiles (1, 2, 3, 4) with $\delta/h = 0{,}2\ and\ a = 1\,[m]$.

It is interesting to note from Fig. 15 b) that when a certain value of the load force F is applied, the deflection at the right end becomes zero. Even though we have already seen from Fig. 14 that the maximum deflection is usually at the right free end. This suggests that by only changing the loading value and/or distribution with an educated guess, we can control the value of deformation in the selected position on the beam. Thus, the examples of loading types and beam support types presented in this research are also intended to enable engineers to make educated guesses and recognize patterns. This ultimately aims to improve the efficient utilization of structures predominantly subjected to bending.
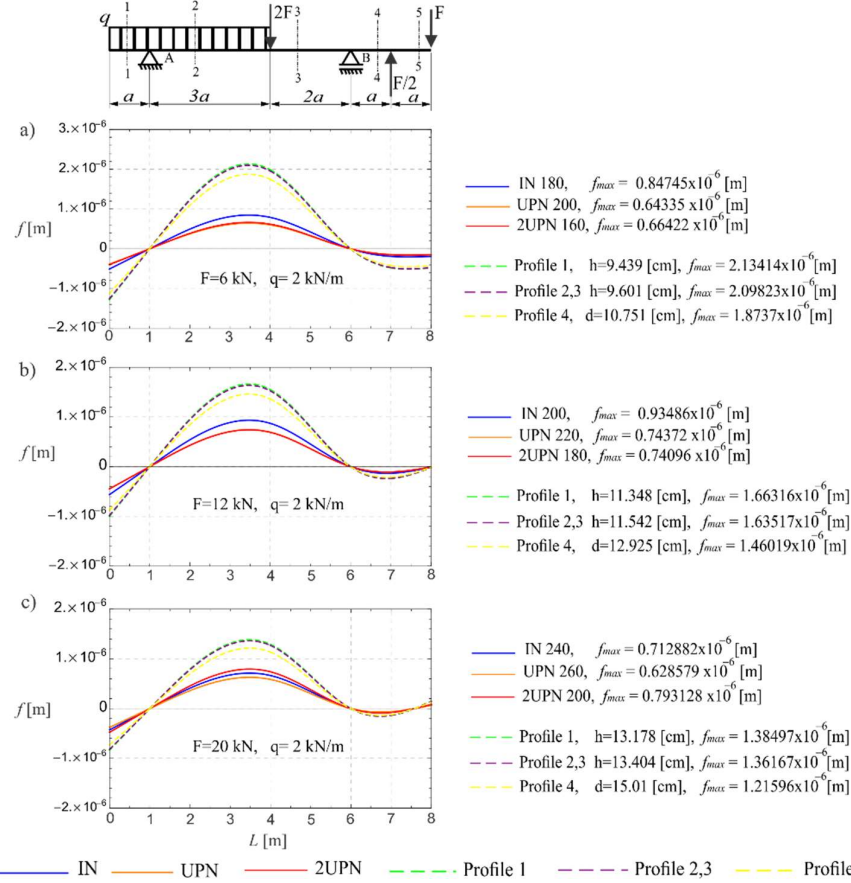
Fig. 15 The elastic curve ($y\,(z) = f\,[m]$) represents the deflection values along the beam length for different scenarios of distributed forces and combinations positive values F at constant continuous loading value $q = 2\,[kN/m]$. The beam has a standard IN, UPN and 2UPN profiles and nonstandard profiles (1, 2, 3, 4) with $\delta/h = 0,2$ and $a = 1\,[m]$.

5. CONCLUSION

The study demonstrates the importance of selecting the optimal cross-sectional shape for beams subjected to bending, based on the theory of elastic bending and the analysis of elastic curves under various loading conditions and boundary scenarios. By deriving the differential equation of the elastic curve and solving it for different beam configurations, we have shown the correlation between beam bending stiffness, shape factor, and the degree of utilization of the cross-sectional shape.

The application of the ultimate bending strength criterion for dimensioning beams has allowed us to determine the characteristic dimensions of profiles according to the

maximum bending moment for each type of beam. The analysis of different cross-sectional profiles under the same loading conditions has provided insights into the maximal deflection and the most efficient profile selection.

Our study demonstrates that the standard I profile is the most optimal cross-sectional shape for beams subjected to bending, considering various parameters such as stiffness, shape factor, and degree of utilization. The analysis shows that the standard I profile has a utilization degree that is 20.75% better than the non-standard U or I profile, making it the preferred choice. Additionally, the standard U profile has a utilization degree that is 12.26% better than the non-standard U or I profile.

When selecting the most favorable profile, the degree of utilization of the profile cross-section provides the characteristic of the best distribution of the cross-sectional area in relation to the neutral axis, the axis around which bending occurs. Ideally, the distant flanges from the axis around which the beam bends are the best in terms of dimensioning the beam according to the criterion of ultimate bending strength. Considering this, we can conclude that the standard I profile is optimal both in terms of stiffness and the utilization of the cross-sectional area, making it the best choice for beams subjected to bending.

Other criteria, such as the allowable maximum deflection value, can also be decisive. Beams with greater stiffness will perform better in dimensioning, having a smaller deflection value for the same load. The shape factor for elastic bending, which gives the ratio of the stiffness of profiles made of the same materials to the stiffness of a solid circular cross-section profile, is also an important consideration.

The findings provide valuable guidance for engineers and designers in selecting the most efficient cross-sectional shapes for beams, ensuring both optimal performance and practical feasibility in structural applications.

The numerical analysis conducted on elastic beams of varying configurations reveals critical insights into their performance under different loading scenarios. The examination included cantilevered beams subjected to continuous and discrete forces, as well as overhanging beams with eccentric loads. By applying the Clebsch procedure, we derived the elastic curves for both standard and non-standard cross-sectional shapes, focusing on maximum bending moments to effectively dimension these profiles.

A key finding is the relationship between profile selection and deflection behavior. Standard profiles consistently exhibit lower maximum deflection values compared to non-standard profiles, establishing their preference in applications where minimal deflection is critical. However, non-standard profiles possess distinctive advantages, particularly in their robustness to small variations in loading. This characteristic allows them to maintain performance stability under fluctuating conditions, making them suitable for situations where load conditions may not be constant.

The analysis also underscores the importance of considering various mechanical and geometric factors during profile selection, such as material efficiency and shape factor. For instance, while standard I profiles often provide superior utilization of cross-sectional areas, non-standard profiles may offer better weight-to-load ratios under specific conditions. Ultimately, the choice of profile must balance these considerations with the specific requirements of the application, factoring in aspects such as allowable deflections and the potential impact of loading eccentricities.

Also, as the applied load on beams increases, the dimensions of the cross-sectional profiles must also expand to ensure structural integrity. This requirement is particularly evident in scenarios involving a significant rise in load, where not only do the height

dimensions marginally increase, but the cross-sectional area can substantially enlarge, leading to a notable weight increase of the beam. For instance, a 2,3-fold increase in load results in a corresponding 50% rise in the beam's weight, highlighting the necessity for designers to consider both structural performance and weight optimization. This balance is crucial, as larger profile dimensions are essential to maintain acceptable deflection levels while coping with increased loading conditions. The various examples of loading and beam support types discussed in this research are designed to help engineers make informed predictions and identify patterns. This approach aims to enhance the efficient use of structures that are primarily subjected to bending.

In summary, this study emphasizes the necessity for engineers to have a comprehensive understanding of the interplay between beam dimensions, loading conditions, and profile selection to optimize structural performance effectively. The observations made provide a valuable framework for future design decisions in structural engineering.

Our upcoming project will focus on integrating and optimizing various input parameters from the mentioned profiles. We will leverage the knowledge gained from elastic lines to seamlessly integrate and optimize additional parameters.

REFERENCES

1. Simonović J., Atanasov Stamenković M., Jovanović B.D., (2025) Interpreting Integration Constants in Elastic Beam Deformation Theory, *Innovative Mechanical Engineering*, Vol.4, No.1, University of Niš, Faculty of Mechanical Engineering, pp.59-84, http://ime.masfak.ni.ac.rs/Dokumenta/papers/v4n1/006_Simonovic_et_al.pdf
2. Bíró, I., Cveticanin, L., & Szuchy, P. (2018). Numerical method to determine the elastic curve of simply supported beams of variable cross section. *Structural Engineering and Mechanics*, 68(6), 713-720. DOI: https://doi.org/10.12989/sem.2018.68.6.713.
3. Fredriksson, C., & Mercier, D. (2019). *Material Properties and Structural Sections*. Ansys Materials Education Division, Level 3 Industrial Case Study. First published September 2019, p. 9, current edition July 2021.
4. Јовановић Д. Б.   и Симоновић Ј. (2023), Отпорност материјала машинских конструкција, универзитетски уџбеник, Машински факултет Универзитета у Нишу, Ниш: Графика Галеб, стр.332, ISBN 978-86-6055-168-1.
5. Јовановић, Б. Д. (2013). *Таблице из отпорности материјала*. Машински факултет Универзитета у Нишу (in Serbian) p. 122